Chemical Engineering Journal 179 (2012) 285–294

Contents lists available at SciVerse ScienceDirect

Chemical Engineering Journal

journal homepage: www.elsevier.com/locate/cej

Direct gas-phase photocatalytic epoxidation of propylene with molecular oxygen by photocatalysts

Van-Huy Nguyen [a], Hsiang-Yu Chan [a], Jeffrey C.S. Wu [a,*], Hsunling Bai [b]

[a] Department of Chemical Engineering, National Taiwan University, Taipei 10617, Taiwan
[b] Institute of Environmental Engineering, National Chiao Tung University, Hsin Chu 300, Taiwan

ARTICLE INFO

Article history:
Received 10 August 2011
Received in revised form 28 October 2011
Accepted 2 November 2011

Keywords:
Epoxidation
Propylene oxide
Photocatalysis
Molecular oxygen
MCM-41
TiO_2

ABSTRACT

The photocatalytic epoxidation of propylene by molecular oxygen is one of the best methods to produce propylene oxide (PO) from the environmental viewpoints. The key is using photo-energy to achieve high PO selectivity and yield at mild conditions. A series of photocatalysts including SiO_2, TiO_2, V-Ti/MCM-41, V_2O_5/SiO_2, Au/TiO_2 and TS-1, were used to evaluate their performance in the photo-epoxidation. The photocatalytic epoxidation of propylene was carried out in the gas mixture of C_3H_6:O_2:N_2 = 1:1:18 at atmospheric pressure. In addition to PO, other products, such as propionaldehyde, acetone, acetaldehyde, ethanol and methanol, were detected. The results indicated that the most favorable photocatalysts for photocatalytic epoxidation were silicates supported group. The highest PO formation rate of 114 μmol g cat^{-1} h^{-1} with selectivity of 47% was obtained over V-Ti/MCM-41 on stream after 4 h at 50 °C and atmospheric pressure under UVA irradiation of 0.2 mW/cm^2. In addition, the selectivity of products was very stable on stream. A possible reaction mechanism was proposed based on the knowledge of species presented during the photocatalytic reaction.

1. Introduction

As the development of third world countries continues, chemicals demand worldwide reaches an unprecedented level. More specifically, the epoxidation of hydrocarbons becomes more important in the industrial production of chemicals, which are used as key intermediates for polymer and organic syntheses. For instant, propylene oxide (PO), the second most important chemical intermediate, has become increasingly important to the chemical industry since 1950s [1–3]. In 1991, the global PO consumption was approximately 3.9 million tons and reached to 6.0 million tons in 2009. Although the global PO consumption has been decreased by 5.6% in 2009 due to economic crisis, it is predicted that average annual growth of over 7% will be seen from 2009 to 2014 as demand recovers [4].

Indeed, there has been great experimental and theoretical studies performed recently focusing on gas-phase propylene epoxidation by using molecular oxygen under high temperature and/or high pressure as shown in Eq. (1).

$$CH_3-CH=CH_2+\frac{1}{2}O_2 \xrightarrow[\text{high temp., high pressure}]{\text{thermocatalyst}} CH_3-\underset{\diagdown\,O\,\diagup}{CH}-CH_2 \quad (1)$$

In 2004, Jin et al. reported that PO selectivity of 60.3% was achieved over the 20%Ag–4%MoO_3/ZrO_2 catalyst under 400 °C, 0.1 MPa and GHSV = 7500 h^{-1} [5]. In 2008, Suo et al. obtained PO selectivity of 17.9% with 0.9% propylene conversion at the initial 10 min of reaction over Au/SiO_2 catalyst at 325 °C, and GHSV = 6000 h^{-1} [6]. The other approaches on exploring the selective catalytic epoxidation of propylene via the mixture of hydrogen and oxygen are shown in Eq. (2).

$$CH_3-CH=CH_2+H_2+O_2 \xrightarrow[\text{high temp., high pressure}]{\text{thermocatalyst}} CH_3-\underset{\diagdown\,O\,\diagup}{CH}-CH_2+H_2O \quad (2)$$

In 2005, Cumaranatunge and Delgass enhanced Au content in Au/TS-1 and achieved 10% conversion, 76% selectivity by using a gas mixture at 473 K [7]. In 2007, the study from Oyama and coworkers achieved a conversion of 1.4%, a PO selectivity of 99%, and a H_2 efficiency of 17% under 423 K and 0.1 MPa by using gold supported on a Ti-containing silicate mesoporous material [8]. The approaches developed for the thermocatalysts by using

* Corresponding author. Tel.: +886 2 23631994; fax: +886 2 23623040.
E-mail address: cswu@ntu.edu.tw (J.C.S. Wu).

1385-8947/$ – see front matter © 2011 Elsevier B.V. All rights reserved.
doi:10.1016/j.cej.2011.11.003

hydrogen–oxygen mixture or only molecular oxygen are very clean and have shown good activity performance. However, the extra energy lost in the reaction, low hydrogen efficiency and safety consideration that requires H_2O_2 production facilities to be restricted in size have made these approaches only a temporary solution.

It is well known that photo-energy is the Earth's ultimate energy source and friendly to environment. Following the excellent pioneer work of Fujishima and Honda in 1972 [9], scientific and engineering interests in TiO_2, particularly in the field of photocatalysis, have grown significantly [10–16]. However, there are only few researches on photo-epoxidation in the presence of photocatalysts and their performances are not advanced yet [17–23]. In 2000, Yoshida et al. investigated more than 50 types of silica-supported metal oxides for their photo-oxidation activities and found that TiO_x/SiO_2 was the most effective photocatalyst attaining 4.7% in PO yield and 19.2% in PO selectivity under batch reaction with 200 W Xe lamp irradiation and at 318 ± 5 K [18]. In 2006, Amano et al. proposed V_2O_5 (0.1%)/SiO_2 as the best photocatalyst until now, which has demonstrated a PO formation rate of 85 μmol g cat^{-1} h^{-1} and a PO selectivity of 37% under continuous reaction at 303 K and with UV-C light of 240 < λ < 440 nm [19]. From economic and environmental viewpoints, most of the current studies on epoxidation require further improvements. Although there were two new epoxidation processes developed recently, a cumene–hydroperoxide process (2003 in Japan) and a hydrogen peroxide (H_2O_2) epoxidation process (2008 in Belgium), they still based on multi-stage liquid-phase reactions and required hydrogen. The photocatalytic epoxidation of propylene is a promising process because it is environmentally friendly, and the process can be carried out under mild conditions in the absence of hydrogen; however, its performance still needs to be improved.

It is expected that direct epoxidation process to produce PO with the aid of light energy over photocatalysts will be a promising approach for the production of chemicals in the future. Therefore, the main strategy being considered in this study is to develop a direct gas-phase one-pass reaction under mild conditions. Our aim is to explore the selective photocatalytic epoxidation of propylene via an ideal oxidant, i.e., molecular oxygen. The key is using photo-energy to achieve high PO selectivity at mild conditions, as show in Eq. (3).

$$CH_3-CH=CH_2+\frac{1}{2}O_2 \xrightarrow[\text{mild conditions}]{\text{photocatalyst}} CH_3-\underset{\diagdown\,O\,\diagup}{CH}-CH_2 \quad (3)$$

The objective of this study is to evaluate the direct gas-phase photocatalytic epoxidation on a series of photocatalysts such as SiO_2, TiO_2, V-Ti/MCM-41, V_2O_5/SiO_2, Au/TiO_2 and TS-1 at mild conditions. The optimal reaction conditions were also studied for photocatalytic epoxidation by comparing the selectivities and yields of PO for different photocatalysts. The mechanism of photocatalytic epoxidation was also proposed based on the knowledge of species present during the photocatalytic reaction.

2. Experimental

2.1. Preparation of photocatalysts

Titanium dioxide (TiO_2) powder used in this study was commercial P25 (Degussa). The photo-deposition of Au particles on TiO_2 was carried out by the method suggested in the literature [24]. $HAuCl_4$ solution and TiO_2 were mixed together and adjusted to pH 5.5 by using 0.1 M Na_2CO_3 before illumination. The solution was irradiated with a 200 W mercury–arc lamp for 120 min with stirring. The photocatalyst was filtered and washed before drying in an oven at 393 K and calcined in a flow of air at 773 K for 5 h.

Amorphous SiO_2 was prepared from tetraethyl orthosilicate (TEOS, Aldrich, 98%) by using the sol–gel method. The pH of a mixture containing ethanol, TEOS, and deionized water was adjusted to approximately 2 by HCl (0.1 M) solution and the mixture was stirred for 2 h. After that, it was dried in an oven at 393 K and calcined in a flow of air at 973 K for 5 h to yield the amorphous SiO_2 powder.

Titanium silicalite-1 (TS-1) was prepared by the hydrothermal crystallization of gel from tetraethylorthosilicate (TEOS, Aldrich, 98%) and titanium (IV) tetrabutoxide (TBOT, Alfa Aesar, 98%) in the presence of tetrapropylammonium hydroxide (TPAOH, 20% in water, Fluka) with a small amount of polyoxyethylene sorbitan monolaurate (Tween 20), which was reported by Khomane et al. [25]. The ratio of Si to Ti for TS-1 was 19:1 in this study.

V_2O_5 (0.5 wt%)/SiO_2 was prepared using the same method as reported by Amano and Tanaka [26]. First, silicon(IV) oxide (99.5%; Stream chemical) was stirred with an aqueous solution of NH_4VO_3 at 353 K for 2 h, followed by evaporation to dryness. Next, the samples were calcined in dry air at 773 K for 5 h.

Mesoporous V-Ti/MCM-41 molecular sieves were synthesized by simple hydrothermal treatment method using cetyltrimethylammonium bromide (CTAB) as the structure-directing template. The molar composition of the gel mixture was SiO_2:0.01TiO_2:0.01V_2O_5:0.2CTAB:0.89H_2SO_4:120H_2O. In a typical synthesis procedure, 21.2 g of sodium metasilicate monohydrate dissolved in 100 ml DI water was combined with the appropriate amount of metal precursors like titanium oxysulfate hydrate and/or vanadyl sulfate hydrate (dissolved in 20 ml of 2 M H_2SO_4) for the titanium and vanadium sources, respectively. The resulting mixture was stirred vigorously for 30 min. Then, approximately 20 ml of 2 M H_2SO_4 was added to the above mixture to adjust the pH to 10.5 with constant stirring to form a uniform gel. After stirring, the solution containing 7.28 g of CTAB dissolved in 25 ml of DI water was added slowly into the above mixture and the combined mixture was stirred for three additional hours. The resulting gel mixture was transferred into a Teflon coated autoclave and kept in an oven at 145 °C for 36 h. After cooling to the room temperature, the resulting solid was recovered by filtration, washed with DI water and dried in an oven at 110 °C for 8 h. Finally the organic template was removed by calcination at 550 °C for 10 h.

2.2. Characterization

The light absorption of photocatalysts was fully characterized by reflective diffusive UV–vis spectroscopy (UV–vis DRS, Varian Cary 100). $BaSO_4$ was used as a standard reflection reference. Scanning electron microscopy (SEM) was carried out on Nova Nano SEM 230 instrument. Transmission electron microscopy (TEM) was performed on Hitachi H-7100 electron microscope instrument. Powder X-ray diffraction (XRD, Xray-M03XHF, Ultima IV) was used for crystalline structure and calculation of photocatalyst sizes. All peak data measured by XRD analysis were checked and assigned to known crystalline phases by comparing with those of JCPDS database. The X-ray photoelectron spectroscopy (XPS) was carried out to determine the chemical composition of the elements and the chemical status of various species on the Thermo Theta Probe instrument. The specific surface area of photocatalyst was measured by Micrometrics, ASAP 2000. The atomic structure of V-Ti/MCM-41 and TS-1 was studied by X-ray absorption spectroscopy (XAS) at the National Synchrotron Radiation Research Center in Hsin Chu, Taiwan. For Ti K-edge and V K-edge spectra, they were analyzed in fluorescence mode on beam-line 16A. The analysis was performed using ARS DE-202G Closed Cycle Cryostat with Lytle detector. The samples were prepared as powder form, and dispersed on Kapton tape. The

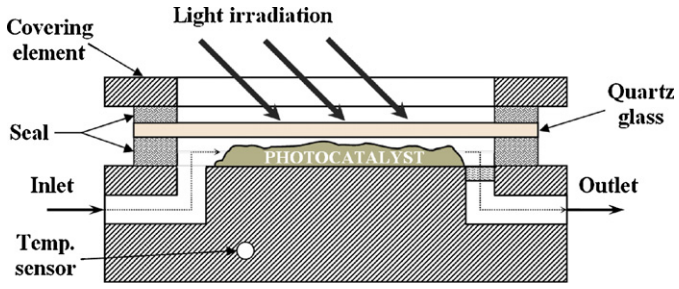

Fig. 1. The scheme of powder packed-bed reactor.

energy step used was 0.2 eV, and the counting time per step was 2 s around the absorption edge.

2.3. Direct gas-phase photocatalytic epoxidation of propylene

All photocatalytic epoxidation experiments were conducted continuously with the reactant gas mixture of C_3H_6:O_2:N_2 = 1:1:18 (controlled by rotameters) at a gas hourly space velocity (GHSV) of 6000 h^{-1} under atmospheric pressure. The photocatalyst (0.02 g) was spread in a powder packed-bed reactor (0.55 cm^3) with a quartz window on top for transmission of light as shown in Fig. 1. The UV-A (wavelength 320–500 nm) from Exfo S1500 (USA) equipped with 200 W mercury–arc lamp was used as the irradiation source and guided to reactor by an optical fiber. The light intensity was measured at the window of the reactor by GOLDILUX Radiometer/Photometer (UV-A Probe/UV-C Probe). The photoreactor was placed on the hot plate in case high-temperature condition was required. The feed gases were analyzed periodically using a gas chromatograph (Young Lin, YL6100 GC) equipped with both a flame ionization detector (FID) and a thermal conductivity detector (TCD). A 6-way valve was used to switch the flow of the sample into the two columns of the GC. A molecular sieve-5A column was used to separate propylene and oxygenates, including PO, propionaldehyde (PA), acetone (AC), acetaldehyde (AA) and alcohol (methanol and ethanol). The Porapak-N on the other hand was used to separate O_2 and CO_2. The following (Eqs. (4–7)) are the definitions of propylene conversion, consumption and adsorption rates, and the selectivity of products for the reaction.

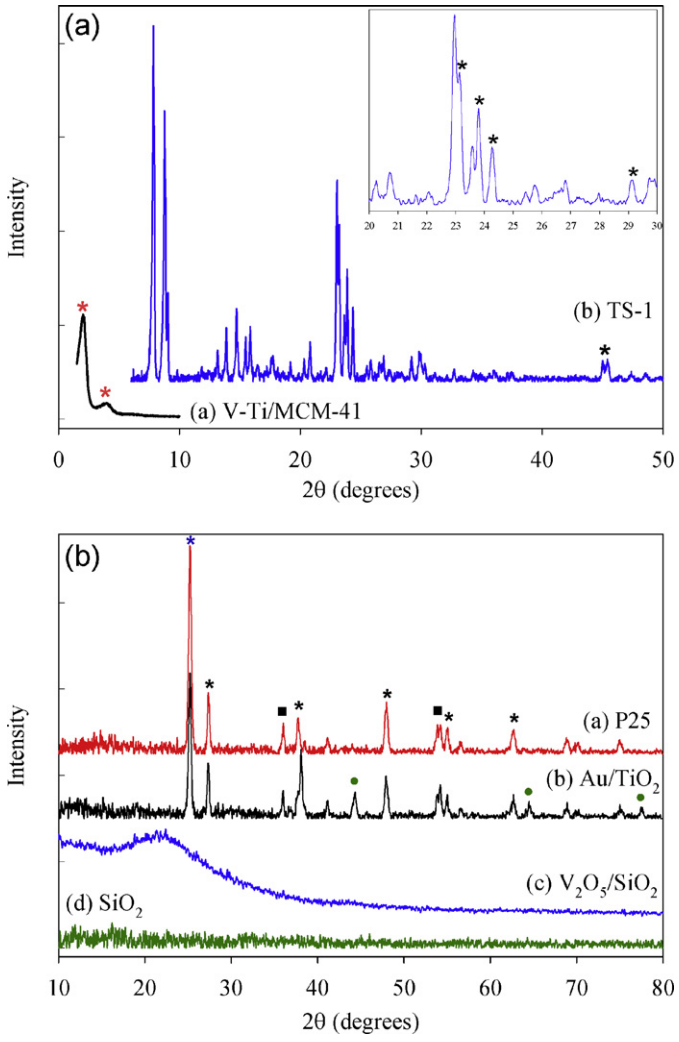

Fig. 2. XRD patterns of different photocatalysts (a) V-Ti-/MCM-41; TS-1 and (b) P25; Au/TiO_2; V_2O_5/SiO_2; SiO_2.

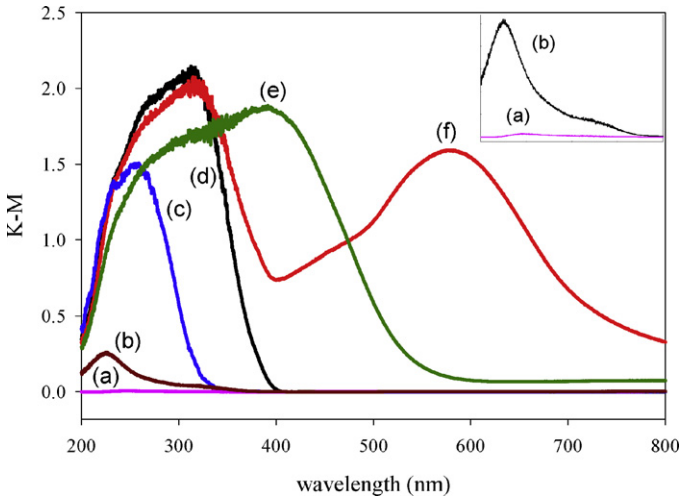

Fig. 3. Diffuse reflectance UV–vis spectroscopy of different photocatalysts (a) SiO_2, (b) V-Ti/MCM-41, (c) TS-1, (d) P25, (e) V_2O_5(0.5 wt%)/SiO_2, and (f) Au(3 wt%)/TiO_2.

$$C_3H_6 \text{ consumption rate} = C_3H_6 \text{feed rate} - C_3H_6 \text{out rate} \quad (4)$$

$$C_3H_6 \text{ conversion rate} = \sum \text{rate of all products covered to C3 products} \quad (5)$$

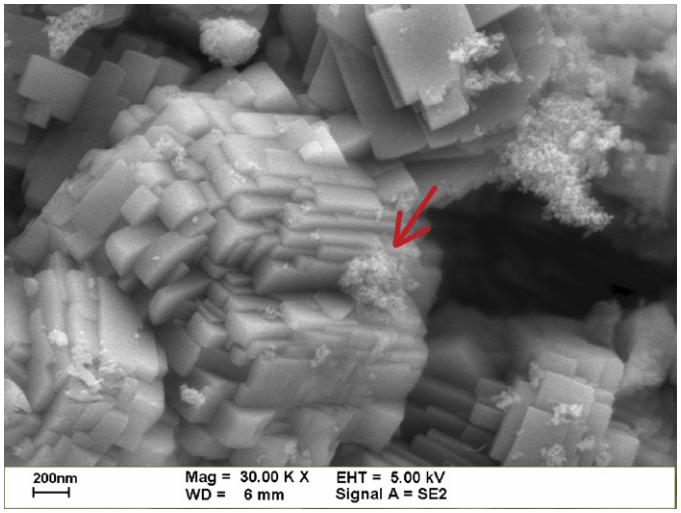

Fig. 4. SEM image of titanium silicalite (TS-1).

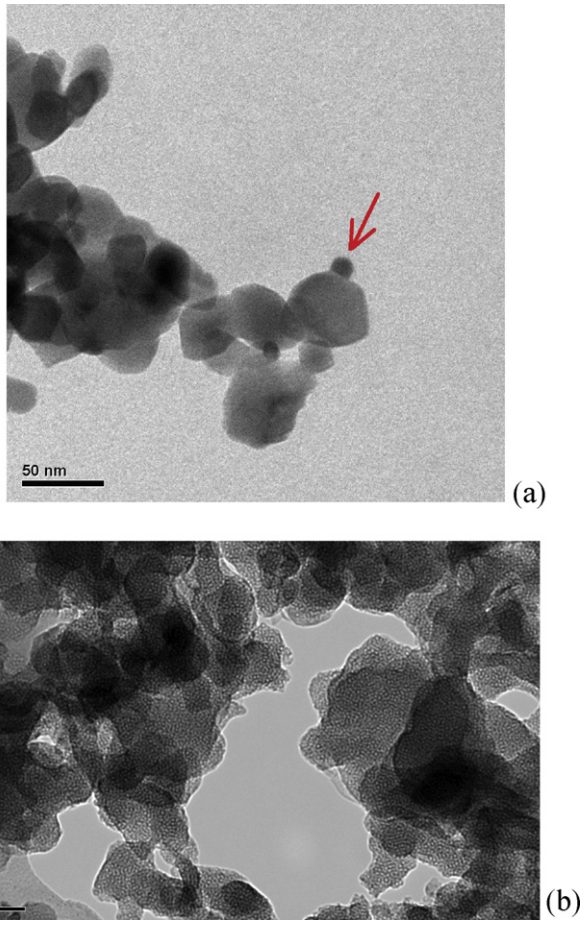

Fig. 5. TEM images of photocatalysts: (a) Au(3 wt%)/TiO_2; and (b) V-Ti/MCM-41.

C_3H_6 adsorption rate

$$= C_3H_6 \text{ consumption rate} - C_3H_6 \text{ conversion rate} \quad (6)$$

Product selectivity

$$= \frac{\text{moles of the formation one C3 product}}{\text{moles of all C3 products}} \times 100\% \quad (7)$$

3. Results and discussions

3.1. Photocatalyst characterization

The X-ray diffraction patterns of various photocatalysts are shown in Fig. 2. As shown in Fig. 2(a), the main diffraction peaks of V-Ti/MCM-41 at $2\theta = 1.9^\circ$ and 3.9° confirm the family of mesopore structure. The diffraction peaks of TS-1, at $2\theta = 23.2^\circ$, 23.8°, 24.3° and 45°, are consistent with the MFI topology structures as shown in the inset of Fig. 2(a) [27]. The presence of single diffractive peaks at $2\theta = 24.3^\circ$ in the XRD pattern indicates a change from monoclinic symmetry (S-1) to orthorhombic symmetry (TS-1) [28]. In Fig. 2(b), the photocatalysts containing TiO_2 showed intensive XRD peaks for anatase phase and rutile phase as expected in P25. Au is highly dispersed on the TiO_2 which exhibits a characteristic XRD pattern with fine structures at $2\theta = 44.38^\circ$, 64.56° and 77.55°. No peak is shown for SiO_2 due to their amorphous structure.

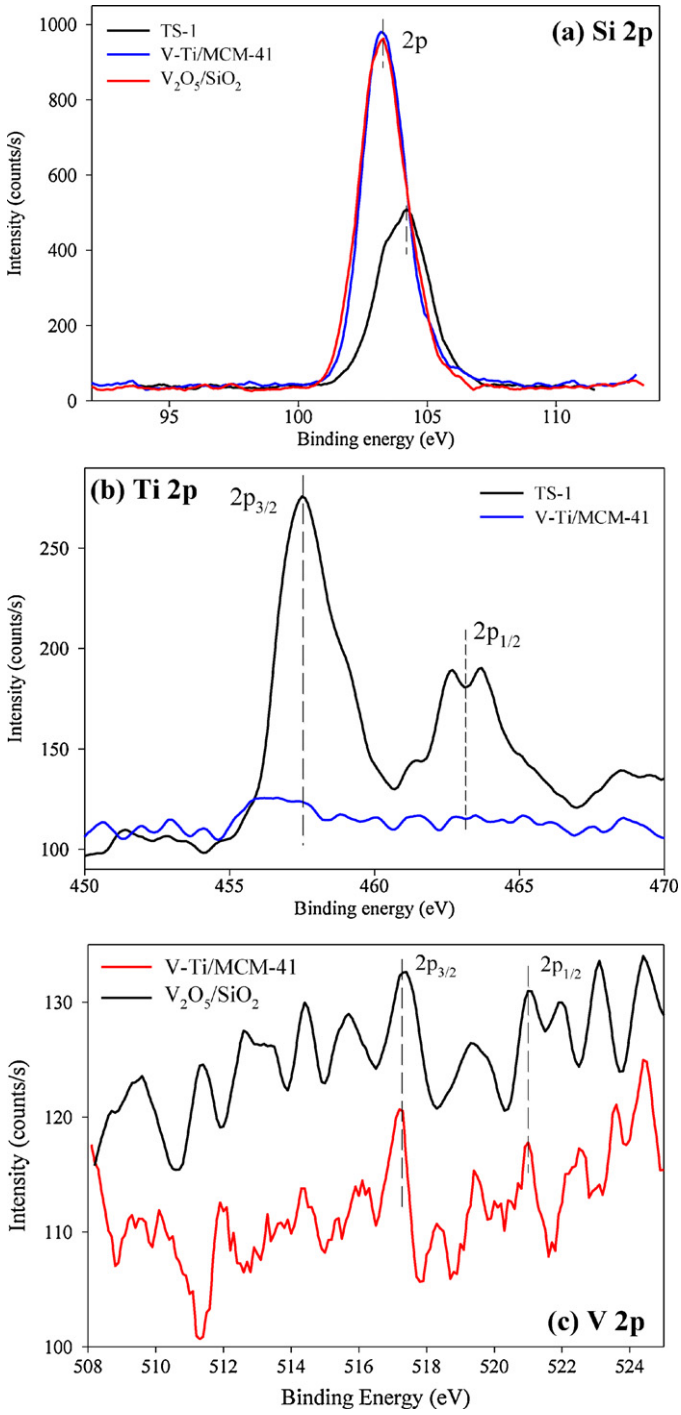

Fig. 6. XPS spectra of: (a) Si 2p: TS-1, V-Ti/MCM-41, V_2O_5/SiO_2; (b) Ti 2p: TS-1, V-Ti/MCM-41 and (c) V 2p: V_2O_5/SiO_2, V-Ti/MCM-41.

Fig. 3 shows the UV–vis diffusive reflectance spectroscopy of different photocatalysts. There is a slight absorption edge at around 200–380 nm for amorphous SiO_2 and V-Ti/MCM-41 as shown in the inset of Fig. 3(a)–(b). The spectrum of TS-1 as shown in Fig. 3(c) is widely used to confirm the electronic transitions between O^{2-} and Ti^{4+} in a tetrahedral environment of isolated framework of Ti(IV) centers. Moreover, the absence of absorption band at 320–400 nm indicates that no anatase or extra framework of Ti is observed in TS-1 [7]. For TiO_2 (P25) shown in Fig. 3(d), the absorption edge is observed at around 400 nm, which is between the absorption edge of anatase (387 nm) and rutile (418 nm). For V_2O_5 (0.5 wt%)/SiO_2

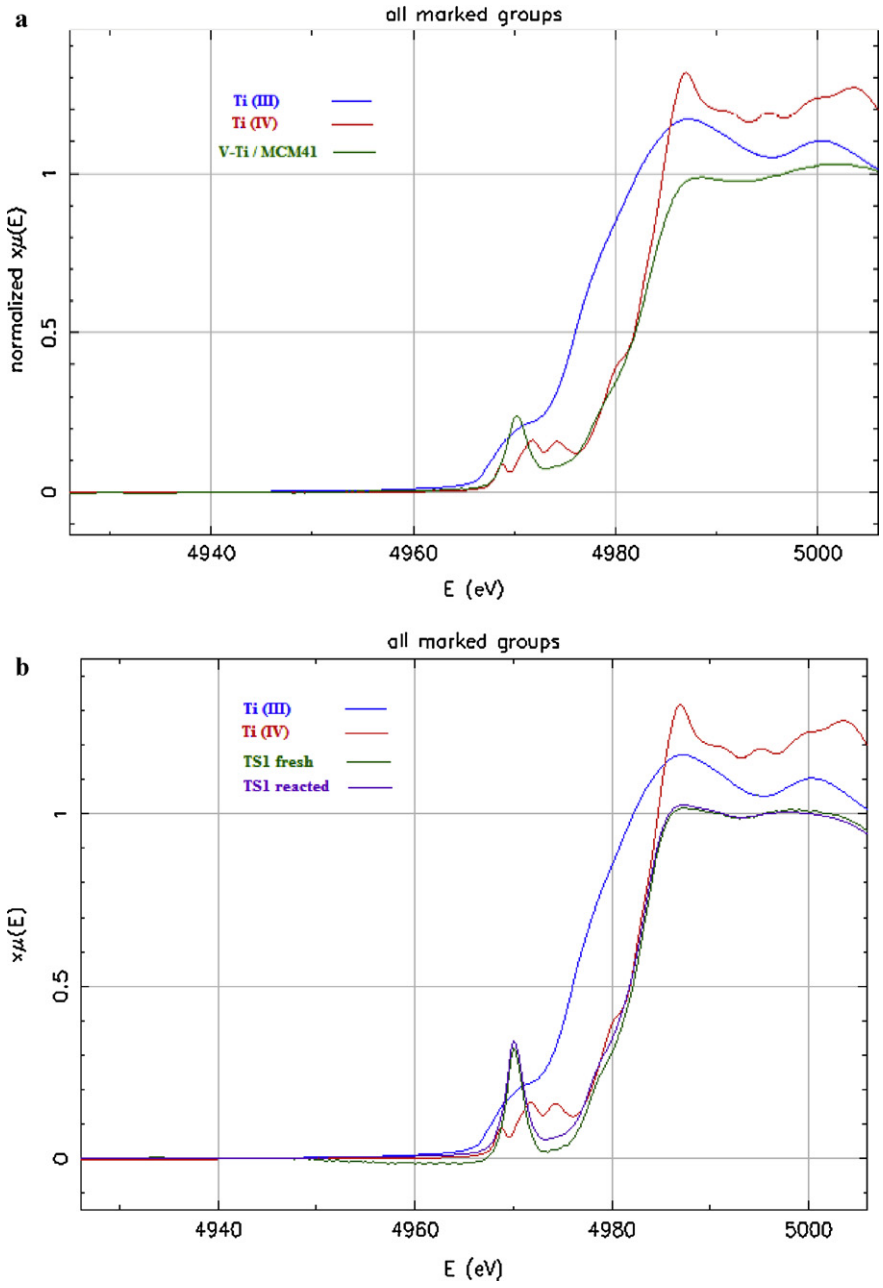

Fig. 7. Summary of the Ti K-edge characterization of (a) V-Ti/MCM-41 and (b) TS-1 by X-ray near edge absorption spectroscopy (XANES).

shown in Fig. 3(e), a ligand–metal-charge-transfer (LMCT) band from O^{2-} to V^{5+} emerges at around 200–550 nm, which is assigned to be a tetrahedral VO_4 monomer [19]. The spectrum of Au/TiO_2 is shown in Fig. 3(f). The Au on TiO_2 significantly affects the light absorption as compared with bare TiO_2, and shows a second absorption band in the visible-light region at ~600 nm, revealing surface plasmonic resonance [29].

Fig. 4 shows the SEM micrograph of TS-1, indicating that a small amount of TiO_2 aggregated on the SiO_2 surface in some regions. Fig. 5(a) and (b) shows the TEM images of Au (3 wt%)/TiO_2 and V-Ti/MCM-41, respectively. The size of Au particles is around 10 nm as shown in Fig. 5(a). With obvious contrast, the nano-structure of MCM-41 can be observed in Fig. 5(b).

Fig. 6(a) shows the binding energies of Si 2p at 103.2 eV and 104.1 eV. The peak of TS-1 at 104.1 eV belongs to silica oxide compound. There is no distinguished shift for V-Ti/MCM-41 and V_2O_5/SiO_2 at 103.2 eV, which indicates that silicates are mainly oxides but hex-fluorosilicate and other anion are also included [30]. Fig. 6(b) shows the binding energies of Ti 2p for TS-1 at 457.5 eV, confirming the presence of Ti^{4+} state. Due to the little amount of Ti on V-Ti/MCM-41, its peak of Ti 2p could not be observed clearly. The Ti state of V-Ti/MCM-41 was confirmed by XAS as shown below. Fig. 6(c) shows the binding energies of V $2p_{3/2}$ and $2p_{1/2}$ for V-Ti/MCM-41 and V_2O_5/SiO_2 at 517.3 eV and 520.9 eV, respectively. The intensities of peaks were closed to background due to the small loading of V_2O_5 (0.5 wt%).

The Ti K-edge X-ray absorption spectroscopy of V-Ti/MCM-41 and TS-1 are shown in Fig. 7. Generally, two kinds of information can be obtained from the X-ray absorption near edge spectroscopy (XANES). The shift of absorption edge indicates the oxidation state

Table 1
Photocatalytic epoxidation of propylene.[a]

Entry	Catalysts	BET surface area ($m^2\ g^{-1}$)[b]	Temp. (°C)	Light intensity (mW/cm^2)	C_3H_6		PO formation rate ($\mu mol\ g^{-1}\ h^{-1}$)	Selectivity (%)[c]					
					Adsorption rate ($\mu mol\ g^{-1}\ h^{-1}$)	Conv. rate ($\mu mol\ g^{-1}\ h^{-1}$)		AA	ROH	PO	PA	AC	CO_2
1	P25	50.0	50	0.2	3444.8	619.5	–	7.6	ND	ND	0.4	17.6	74.4
2	Au (3%)/TiO_2	37.9	50	0.1	2900.9	455.4	4.13	33.7	ND	1.0	5.4	21.7	38.2
3	SiO_2	560.1	50	0.1	2113.6	4.5	0.21	77.3	ND	10.6	12.1	ND	ND
4	V_2O_5 (0.5%)/SiO_2		50	0.2	1459.9	26.1	–	49.9	ND	ND	50.1	ND	ND
5	TS-1	368.9	25	0.2	59.6	25.4	1.31	31.6	ND	24.1	ND	ND	44.3
			50	0.2	3886.7	50.7	19.69	29.0	0.9	40.1	22.9	7.1	trace
			50	0.1	521.9	55.7	24.08	15.9	ND	44.7	32.3	7.0	trace
			70	0.1	n.s.	59.7	17.91	38.3	ND	31.0	24.6	6.1	trace
			50	0.05	n.s.	16.9	5.02	38.5	ND	33.2	16.6	12.0	trace
6	V-Ti/MCM-41	790	50	0.2	11972.5	243.5	114.18	21.3	ND	46.8	26.2	5.7	ND
			25	0.2	n.s.	163.1	54.52	41.4	2.3	32.0	17.8	6.5	ND
			75	0.2	2013.6	223.2	87.92	22.0	1.7	40.2	26.9	9.2	ND
			120	0.2	13624.9	207.5	81.96	11.8	ND	39.6	45.1	3.5	ND
			50	0.4	9323.8	283.0	92.80	24.3	1.4	33.2	22.6	18.5	ND
			50	0.1	12915.6	121.8	48.35	21.1	ND	40.1	29.8	9.0	ND

ND: not detected by GC.
[a] Reaction conditions: photocatalyst 0.02 g; feed gas C_3H_6:O_2:N_2 = 1:1:18 vol% at a gas hourly space velocity (GHSV) of 6000 h^{-1}. The data is the mean value obtained on stream after 4 h.
[b] BET surface area was measured by Micromeritics, ASAP 2000.
[c] PO: propylene oxide; PA: propionaldehyde; AC: acetone; AA: acetaldehyde; ROH: ethanol and methanol.

of element. The pre-edge peak shows the information of local coordination structure [31]. Compared with the Ti(III) and Ti(IV), the average oxidation state of titanium in V-Ti/MCM-41 and TS-1 should be Ti^{4+} from the shifts of absorption edges shown in Fig. 7(a) and (b), respectively. From the pre-edge peaks of Fig. 7(a), the local coordination structure of Ti^{4+} is suggested to be tetrahedral. As shown in Fig. 7(b), the pre-edge peak of TS-1_fresh is higher than that of TS-1_reacted. The local coordination structure of TS-1_fresh is close to genuine tetrahedral while that of TS-1_reacted is slightly distorted. This suggests that TS-1 is distorted due to Ti connecting to propylene or other oxygenates during reaction.

3.2. Direct gas-phase photocatalytic epoxidation of propylene

Table 1 summarizes the results of photocatalytic epoxidation of propylene with oxygen over a series of photocatalysts in a continuous packed-bed reactor at mild conditions. The conversion rates of propylene range from 4.5 to 619.5 $\mu mol\ g\ cat^{-1}\ h^{-1}$ while PO selectivity ranges from 1% to 46.8%. In addition to PO, other products, such as propionaldehyde, acetone, acetaldehyde, ethanol and methanol were detected and their selectivities were calculated. The most dramatic differences between two supported photocatalysts (TiO_2 and SiO_2) are in the production of side products and the

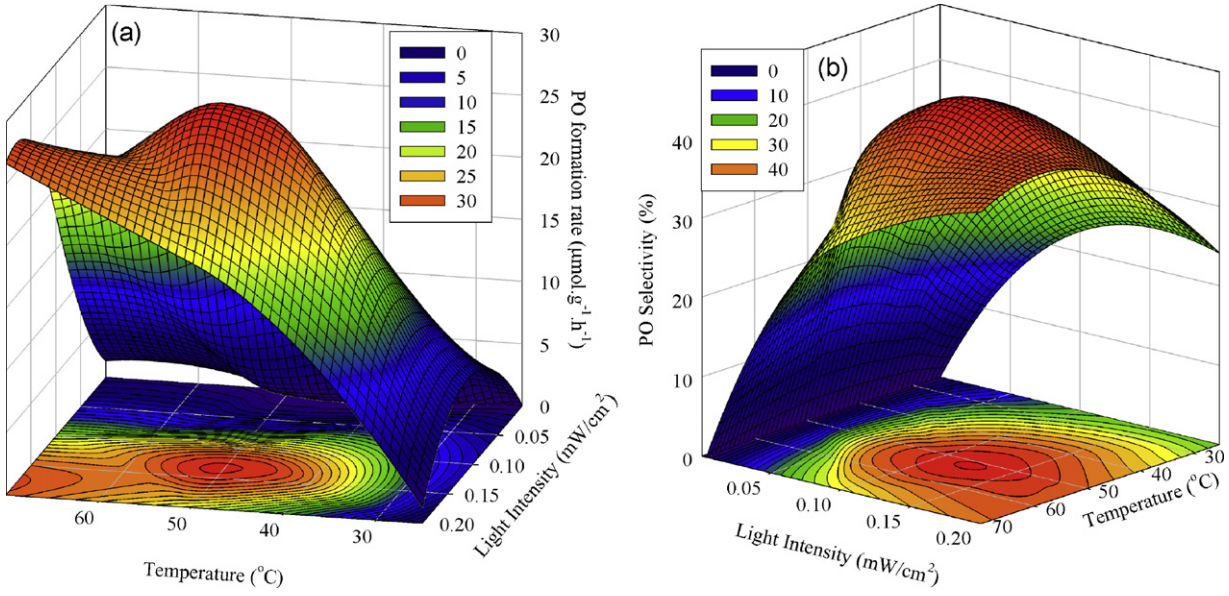

Fig. 8. The effective light of intensity and temperature for photocatalytic epoxidation over TS-1: (a) PO formation rate and (b) PO selectivity.

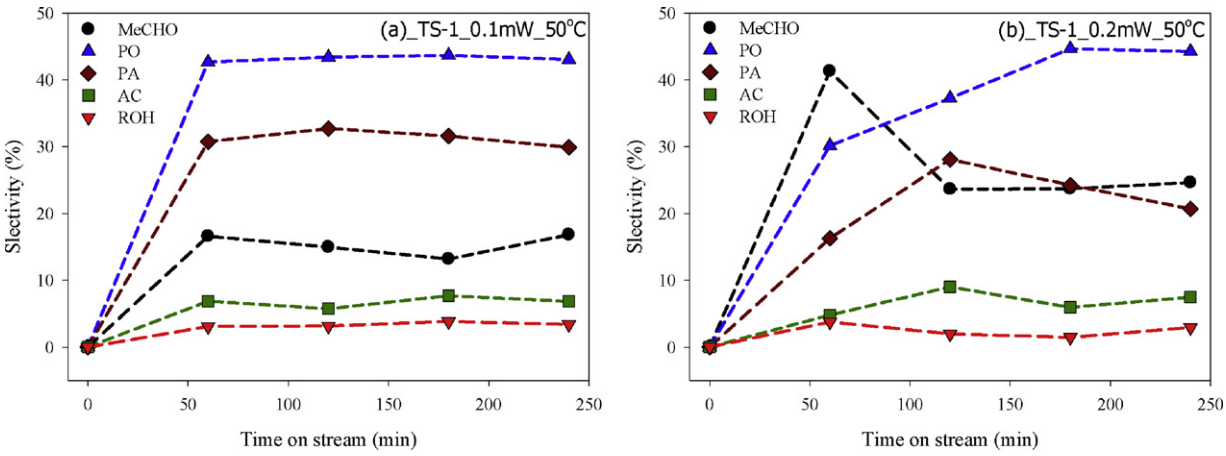

Fig. 9. The time-dependent behavior of selectivity for the formation of PO (▲), PA (♦), AC (■), ROH (▼) and MeCHO (●) on stream over TS-1 under different light intensity conditions: (a) 0.1 mW/cm^2 and (b) 0.2 mW/cm^2.

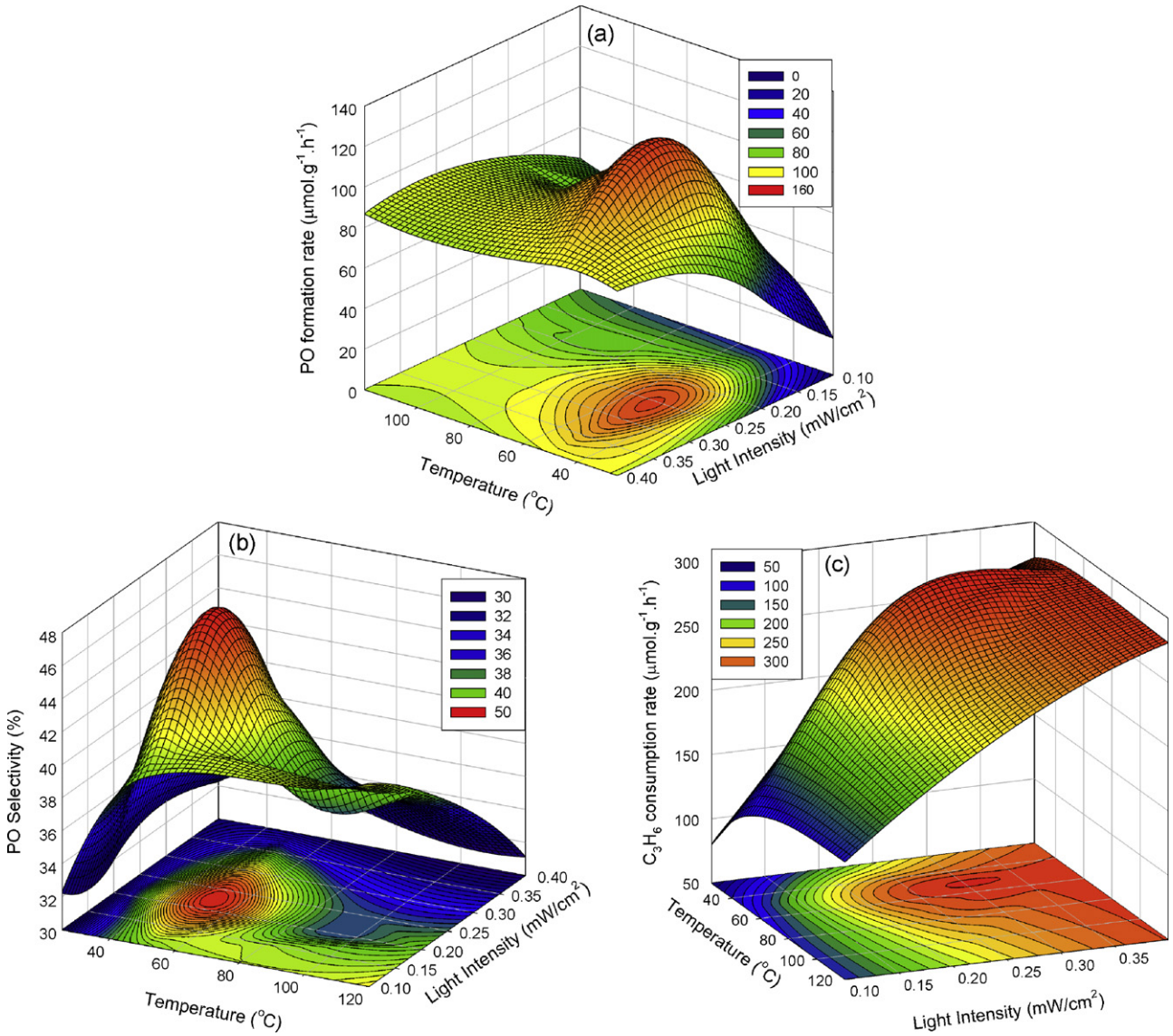

Fig. 10. The effects of light intensity and temperature on the photocatalytic epoxidation over V-Ti/MCM-41: (a) PO formation rate (b) PO selectivity and (c) C_3H_6 conversion rate.

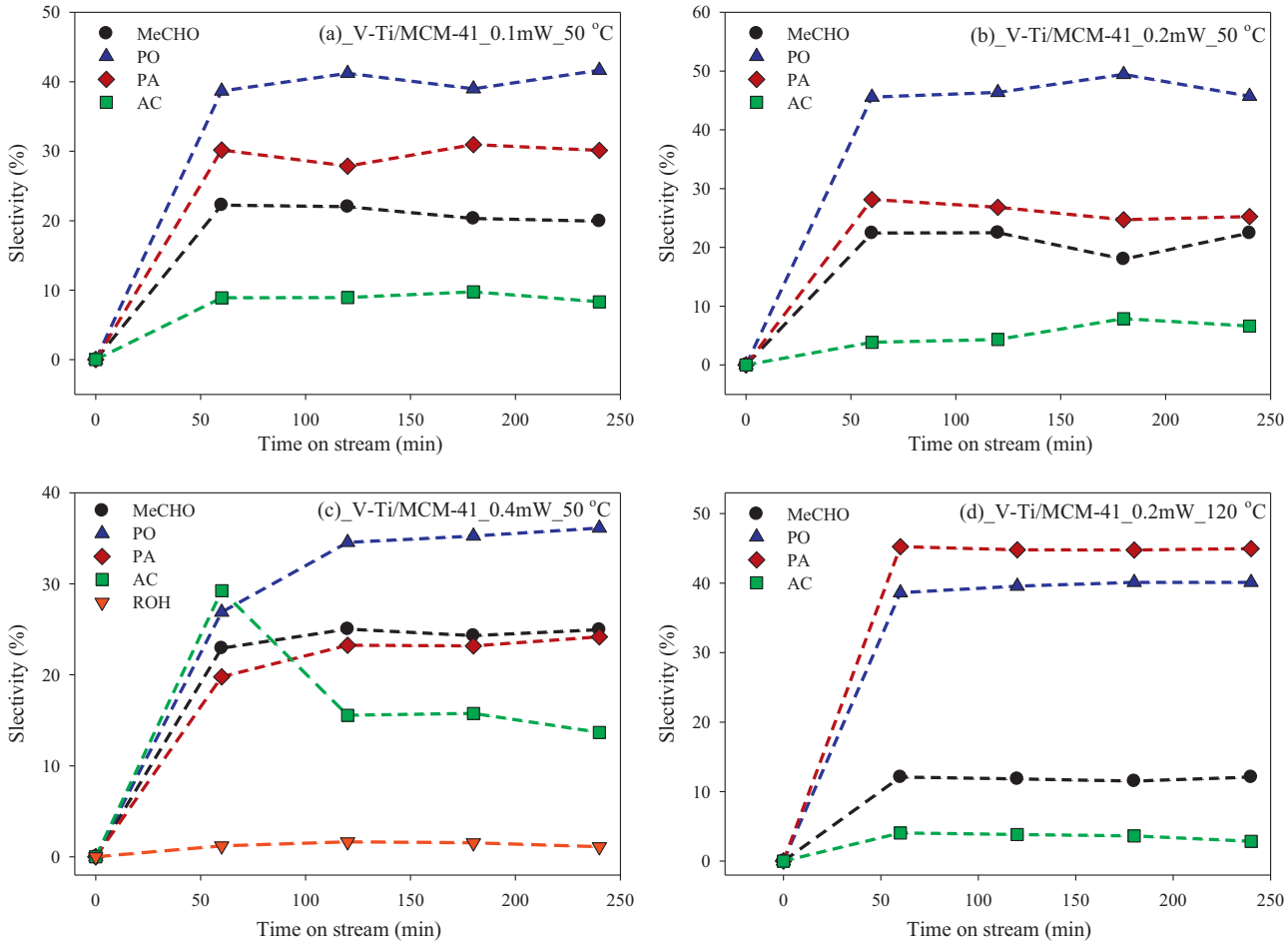

Fig. 11. The time-dependent behavior of selectivity for the formation of PO (▲), PA (♦), AC (■), ROH (▼) and MeCHO (●) over V-Ti/MCM-41 at different conditions: (a) 0.1 mW/cm^2, 50 °C; (b) 0.2 mW/cm^2, 50 °C; (c) 0.4 mW/cm^2, 50 °C and (d) 0.2 mW/cm^2, 120 °C.

conversion rate of C_3H_6. TiO_2 support can convert more C_3H_6 to total oxidation while SiO_2 support leads to low oxidation at lower C_3H_6 conversion.

The adsorption of propylene was observed for all photocatalysts during photoreaction after switching on the UV light. Table 1 lists the average adsorption rates based on the carbon balance in 4 h reaction. The propylene adsorption is the combination of physical and chemical adsorptions on the supports, which depends on surface area and TiO_2 content. The amount of propylene adsorbed on V-Ti/MCM41 was substantial because of the mesoporous nature of material.

Commercial TiO_2 (entry 1) shows high photo-oxidation activity. The C_3H_6 consumption rate is 619.5 μmol g^{-1} h^{-1} with most CO_2 in the products, and no PO is observed. The size of Au particles is very important on epoxidation. This study also confirms that the Au particle with size higher than 5.0 nm prefers complete oxidation of C_3H_6 to CO_2 as shown in entry 2 [32]. A considerable amount of CO_2 is produced not only from the direct photo-oxidation of propylene, but also from the successive photo-oxidation of oxygenated products. Hence, only a few PO can be generated over Au/TiO_2 and TiO_2.

The UV absorption of amorphous SiO_2 is very low (Fig. 3), thus very low C_3H_6 conversion rate was obtained as listed in entry 3 of Table 1. However, the selectivity to form PO still can reach 10.6%. The main reason may be the high specific surface area of SiO_2, 560.1 m^2 g cat^{-1}. Therefore, SiO_2 can harvest more photo-energy in order to produce sufficient electron–hole pairs on the photocatalyst and carry out partial oxidation successfully. The dispersed vanadium oxide on silica had significantly improved the light absorption at around 200–550 nm (Fig. 3). As listed in entry 4 of Table 1, PO still cannot be produced over V_2O_5/SiO_2 although the C_3H_6 conversion rate increased 5 times as compared with amorphous SiO_2.

The most favorable photocatalytic epoxidation was on TS-1 and V-Ti/MCM-41 under various reaction conditions as shown in entry 5 and 6 of Table 1, respectively. These two photocatalysts

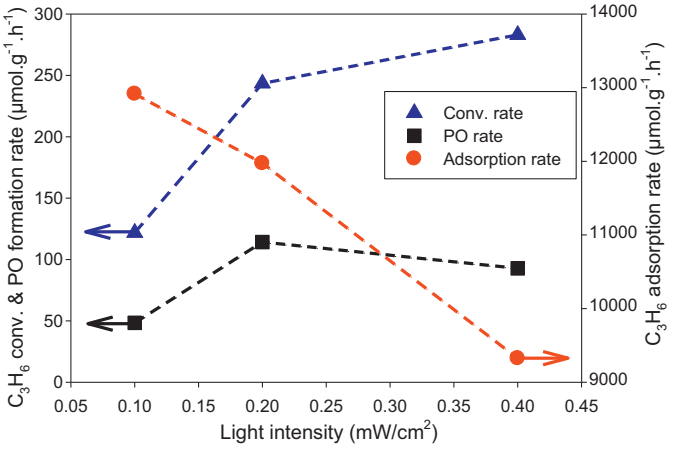

Fig. 12. The light effect on PO formation, C_3H_6 conversion and C_3H_6 adsorption rate for V-Ti/MCM-41.

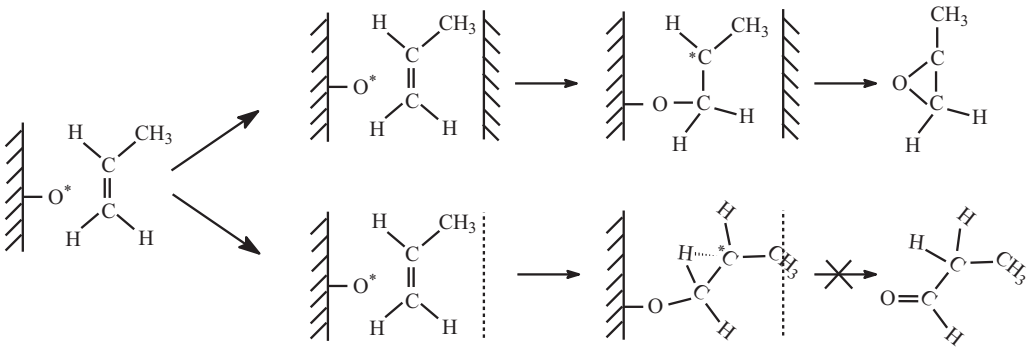

Fig. 13. The formation mechanism of PO and oxygenate products over V-Ti/MCM-41 photocatalyst.

prepared from SiO_2 supported materials are all active and stable for the production of PO, despite having significantly different optimal conditions. For instance, the highest PO formation rate of 114.18 μmol g cat^{-1} h^{-1} with selectivity of 46.8% was observed for V-Ti/MCM-41at 50 °C under light intensity of 0.2 mW/cm^2.

The photocatalytic epoxidation over TS-1 was studied at different light intensities and temperatures as shown in Fig. 8. The optimum conditions of 0.1–0.15 mW/cm^2 and 40–50 °C were found which can achieve the highest PO formation rate and selectivity. Further investigations on time-dependent behavior of PO selectivity are shown in Fig. 9. The stable selectivities of products are achieved under the light intensity of 0.1 mW/cm^2 as shown in Fig. 9(a). The XANES (Fig. 7(b)) revealed that the oxidation states of the Ti species are the same before and after reaction. Therefore, stable active sites can be maintained during photocatalytic epoxidation. However, the selectivities are unstable with higher light intensity as shown in Fig. 9(b). When higher light intensity is supplied, more elections and holes are generated on the photocatalyst. Thus more active intermediate oxygenates may be generated resulting in unstable selectivities.

V-Ti/MCM-41 exhibited excellent selectivity for the photo-epoxidation of propylene with molecular oxygen. Fig. 10 shows the light and temperature effects on photocatalytic epoxidation for V-Ti/MCM-41. Light intensity and temperature have significant impacts on photocatalytic epoxidation and there exists an optimum condition in the range of 0.2–0.3 mW/cm^2 and 40–60 °C as revealed in Fig. 10(a). V-Ti/MCM-41 has much lower UV–vis absorption edge than TS-1 (Fig. 3). Hence, increase in light intensity can significantly enhances the C_3H_6 conversion rate as shown in Fig. 10(c). However, oversupply of light would eventually reduce the selectivity and formation rate of PO as shown in Fig. 10(a) and (b).

Compare to TS-1, V-Ti/MCM-41 also shows a quite similar time-dependent behavior in PO selectivity for the photocatalytic epoxidation. However, as shown in Fig. 11, V-Ti/MCM-41 holds stable selectivities on stream within a wide range of light intensity, 0.1–0.4 mW/cm^2, while TS-1 can only maintain stable selectivities at the light irradiation of 0.1 mW/cm^2. The possible reason is that V-Ti/MCM-41 has the lower UV–vis light absorption than TS-1, hence more photo-energy is required than TS-1. Although PO is still the dominant product with increasing light intensity, a slight increase in acetone and alcohol concentration is observed at 50 °C (Fig. 11(a)–(c)). Increasing temperature to 120 °C substantially increases the amount of propionaldehyde produced while that of PO remains at the same level (Fig. 11(d)).

Fig. 12 shows the influence of light intensity on PO formation, C_3H_6 conversion and C_3H_6 adsorption rate over V-Ti/MCM-41. The adsorption rate of C_3H_6 is significant on V-Ti/MCM-41 due to its porous structure. The adsorption rate decreases noticeably with increase in light intensity. Increasing light intensity enhances the C_3H_6 conversion rate thus also increases PO formation rate. However, further increasing light intensity inhibits PO selectivity. Hence, the PO formation rate starts to decline after reaching an optimum PO formation rate at 0.2 mW/cm^2.

3.3. Proposed mechanism of photocatalytic epoxidation

The intrinsic epoxidation mechanism is still not quite clear. A possible reaction mechanism is proposed based on the knowledge of species present during the photocatalytic reaction. A pair of negative electron (e^-) and positive hole (h^+) is formed in the photocatalyst with light irradiation as in Eq. (8).

$$\text{photocatalyst} \xrightarrow{h\nu} e^- + h^+ \tag{8}$$

Gas-phase O_2 is adsorbed and becomes O_2^- when react with an electron as shown in Eq. (9).

$$O_{2(g)} + e^- \rightarrow O_{2(ads)}{}^- \tag{9}$$

The species $O_{2(ads)}{}^-$ is stable and not directly active in this process. Hence, the active species, surface atomic oxyradicals, are formed by the reaction of the preceding species with the positive hole as shown in Eq. (10).

$$O^-_{2(ads)} + h^+ \rightarrow 2O_{(ads)}{}^* \tag{10}$$

In the epoxide reaction, there are several pathways to create the products. For example, the above surface atomic oxyradicals $O_{(ads)}{}^*$ can react with propylene to yield 3 kinds of products (~80–90% for all products) as listed in Eq. (11).

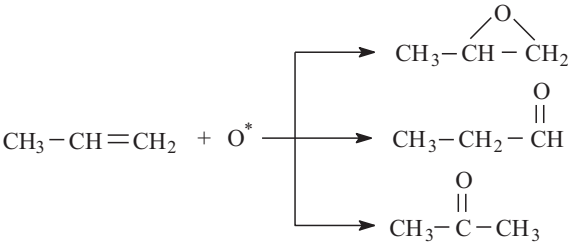

(11)

Carter and Goddard [33] proposed the selective oxidation mechanism of propylene to epoxide via H-atom abstraction by forming oxypropenyl intermediate. The product selectivities depend on the angle of H-atom abstraction from the propylene attacked by $O_{(ads)}{}^*$ and the reaction conditions. Fig. 13 displays the mechanism to create intermediate species of PO and another product via H-atom abstraction in a limited space, e.g. inside pore. The oxypropenyl intermediate of PO is favorable inside the pore while that of propionaldehyde cannot be formed due to space limitation. Therefore, we suggested that the selectivity of PO could be increased due to the pore restriction of MCM-41.

4. Conclusions

A direct photo epoxidation process to produce PO from propylene by O_2 with the aid of light energy over photocatalysts is a promising technology for the production of chemicals in the near future. Compared to other thermal processes of propylene epoxidation, no hydrogen is required in the photocatalytic process. Furthermore, sunlight may be applied in the photo-epoxidation in the future. In this study, under mild conditions, Ti-V/MCM-41 and TS-1 promote the photocatalytic epoxidation of propylene with molecular oxygen at steady state in a flow reactor system. The highest PO formation rate and PO selectivity achieved on stream after 4 h over Ti-V/MCM-41 is 114 μmol g cat^{-1} h^{-1} and 47%, respectively, at 50 °C and atmospheric pressure. In summary, V-Ti/MCM-41 is the most favorable photocatalyst for the photocatalytic epoxidation in this study, and the selectivity of PO could be further enhanced possibly by solving the pore restriction of reaction intermediate.

Acknowledgment

We gratefully acknowledge the National Science Council of Taiwan for financial supporting this research under contract numbers,NSC 99-2923-E-002-002-MY2 and NSC 99-2221-E-009-037-MY3.

References

[1] K. Weissermel, H.-J. Arpe, C.R. Lindley, Industrial Organic Chemistry, 4th illustrated ed., Wiley-VCH, 2003, pp. 265–276.
[2] T.A. Nijhuis, M. Makkee, J.A. Moulijn, B.M. Weckhuysen, Industrial and Engineering Chemistry Research 45 (2006) 3447–3459.
[3] D. Kahlich, U. Wiechern, J. Lindner, Propylene Oxide, in: Ullmann's Encyclopedia of Industrial Chemistry, John Wiley & Sons Inc, 2009, pp. 21355–21379.
[4] WP Coverage of Propylene Oxide, 2010.
[5] G. Jin, G. Lu, Y. Guo, Y. Guo, J. Wang, X. Liu, Catalysis Today 93–95 (2004) 173–182.
[6] Z. Suo, M. Jin, J. Lu, Z. Wei, C. Li, Journal of Natural Gas Chemistry 17 (2008) 184–190.
[7] L. Cumaranatunge, W.N. Delgass, Journal of Catalysis 232 (2005) 38–42.
[8] J. Lu, X. Zhang, J.J. Bravo-Suárez, K.K. Bando, T. Fujitani, S.T. Oyama, Journal of Catalysis 250 (2007) 350–359.
[9] A. Fujishima, K. Honda, Nature 238 (1972) 37–38.
[10] Y.-H. Yu, Y.-T. Pan, Y.-T. Wu, J. Lasek, J.C.S. Wu, Catalysis Today 174 (2011) 141–147.
[11] S. Cao, K.L. Yeung, P.-L. Yue, Applied Catalysis B: Environmental 76 (2007) 64–72.
[12] J. Wu, C.-W. Huang, Frontiers of Chemical Engineering in China 4 (2010) 120–126.
[13] A.J. Maira, W.N. Lau, C.Y. Lee, P.L. Yue, C.K. Chan, K.L. Yeung, Chemical Engineering Science 58 (2003) 959–962.
[14] T.-V. Nguyen, J.C.S. Wu, Applied Catalysis A: General 335 (2008) 112–120.
[15] T.-V. Nguyen, J.C.S. Wu, Solar Energy Materials and Solar Cells 92 (2008) 864–872.
[16] K.L. Yeung, W.K. Leung, N. Yao, S. Cao, Catalysis Today 143 (2009) 218–224.
[17] C. Murata, H. Yoshida, J. Kumagai, T. Hattori, Journal of Physical Chemistry B 107 (2003) 4364–4373.
[18] H. Yoshida, C. Murata, T. Hattori, Journal of Catalysis 194 (2000) 364–372.
[19] F. Amano, T. Yamaguchi, T. Tanaka, Journal of Physical Chemistry B 110 (2006) 281–288.
[20] V.-H. Nguyen, J.C.S. Wu, Photocatalytic epoxidation of propylene with molecular oxygen by photocatalysts, in: 28th Taiwan Symposium of Catalysis and Reaction Engineering, Taipei, Taiwan, 2010, Abtract book, p. 48.
[21] H. Yoshida, C. Murata, T. Hattori, Chemical Communication (1999) 1551–1552.
[22] H. Yoshida, T. Tanaka, M. Yamamoto, T. Funabiki, S. Yoshida, Chemical Communication (1996) 2125–2126.
[23] H. Kanai, M. Shono, K. Hamada, S. Imamura, Journal of Molecular Catalysis A: Chemistry 172 (2001) 25–31.
[24] Y.-F. Yang, P. Sangeetha, Y.-W. Chen, International Journal of Hydrogen Energy 34 (2009) 8912–8920.
[25] R.B. Khomane, B.D. Kulkarni, A. Paraskar, S.R. Sainkar, Materials Chemistry and Physics 76 (2002) 99–103.
[26] F. Amano, T. Tanaka, Catalysis Communications 6 (2005) 269–273.
[27] B.F. Mentzen, F. Lefebvre, Comptes Rendus de l'Académie des Sciences – Series IIC – Chemistry 3 (2000) 843–847.
[28] L. Wang, Y. Zhou, Z. Mi, Journal of Chemical Technology and Biotechnology 82 (2007) 414–420.
[29] J.-J. Chen, J.C.S. Wu, P.C. Wu, D.P. Tsai, Journal of Physical Chemistry C 115 (2010) 210–216.
[30] J.F. Moulder, J.E. Chastain, Handbook of X-ray Photoelectron Spectroscopy: A Reference Book of Standard Spectra for Identification and Interpretation of XPS Data, Perkin-Elmer Corporation, Physical Electronics Division, Eden Prairie, MN, 1992, pp. 56–57.
[31] T. Maschmeyer, F. Rey, G. Sankar, J.M. Thomas, Nature 378 (1995) 159–162.
[32] S.T. Oyama, Mechanisms in Homogeneous and Heterogeneous Epoxidation Catalysis, 1st ed., Elsevier, Amsterdam, Boston, 2008, Chapter 11, pp. 315–338.
[33] E.A. Carter, W.A. Goddard, Journal of Catalysis 112 (1988) 80–92.